Canopy nitrogen, carbon assimilation, and albedo in temperate and boreal forests: Functional relations and potential climate feedbacks

S. V. Ollinger[a,1], A. D. Richardson[a], M. E. Martin[a], D. Y. Hollinger[b], S. E. Frolking[a], P. B. Reich[c], L. C. Plourde[a], G. G. Katul[d], J. W. Munger[e], R. Oren[d], M.-L. Smith[b,f], K. T. Paw U[g], P. V. Bolstad[c], B. D. Cook[c], M. C. Day[a], T. A. Martin[h], R. K. Monson[i], and H. P. Schmid[j]

[a]Complex Systems Research Center, Institute for the Study of Earth, Oceans, and Space, University of New Hampshire, Durham, NH 03824; [b]U.S. Department of Agriculture Forest Service, Northern Research Station, Durham, NH 03824; [c]Department of Forest Resources, University of Minnesota, St. Paul, MN 55108; [f]U.S. Department of Agriculture Forest Service, Legislative Affairs, Washington, DC 20250; [d]Nicholas School of the Environment and Earth Sciences, Duke University, Durham, NC 27708; [h]School of Forest Resources and Conservation, University of Florida, Gainesville, FL 32611; [i]Department of Ecology and Evolutionary Biology, University of Colorado, Boulder, CO 80309; [e]Department of Earth and Planetary Sciences, Harvard University, Cambridge, MA 02138; [g]Department of Land, Air, and Water Resources, University of California, Davis, CA 95616; and [j]Institute of Meteorology and Climate Research, Forschungszentrum Karlsruhe, 82467 Garmisch-Partenkirchen, Germany

Communicated by William H. Schlesinger, Cary Institute of Ecosystem Studies, Millbrook, NY, October 7, 2008 (received for review September 8, 2008)

The availability of nitrogen represents a key constraint on carbon cycling in terrestrial ecosystems, and it is largely in this capacity that the role of N in the Earth's climate system has been considered. Despite this, few studies have included continuous variation in plant N status as a driver of broad-scale carbon cycle analyses. This is partly because of uncertainties in how leaf-level physiological relationships scale to whole ecosystems and because methods for regional to continental detection of plant N concentrations have yet to be developed. Here, we show that ecosystem CO_2 uptake capacity in temperate and boreal forests scales directly with whole-canopy N concentrations, mirroring a leaf-level trend that has been observed for woody plants worldwide. We further show that both CO_2 uptake capacity and canopy N concentration are strongly and positively correlated with shortwave surface albedo. These results suggest that N plays an additional, and overlooked, role in the climate system via its influence on vegetation reflectivity and shortwave surface energy exchange. We also demonstrate that much of the spatial variation in canopy N can be detected by using broad-band satellite sensors, offering a means through which these findings can be applied toward improved application of coupled carbon cycle–climate models.

nitrogen cycle | climate change | foliar nitrogen | ecosystem-climate feedback | remote sensing

Terrestrial ecosystems influence the Earth's climate through regulation of mass and energy exchange with the atmosphere. In recent years, much of the focus has been directed toward factors affecting the ≈1- to 2-Pg carbon (C) sink that is believed to exist in the terrestrial biosphere (1). Candidate mechanisms include forest regrowth after agricultural abandonment (2) and growth enhancement from nitrogen (N) deposition and/or elevated CO_2 (3, 4). In each case, interactions between C and N play a central role. Observations of N limitations to productivity are widespread (5), and responses to experimental CO_2 fertilization are often restricted by N availability (6–8). Although evidence of an N deposition effect on net C exchange has only recently been documented (4), the importance of N as a regulator of C assimilation is well established through the widely observed relationship between leaf-level photosynthetic capacity (A_{max}) and foliar N concentrations (9–11). Despite this understanding, few analyses have included continuous variation in plant N status as a driver of C cycle processes at regional to global scales. There are at least 2 reasons for this. First, because evidence for the photosynthesis–foliar N relationship comes predominantly from leaf-level observations, there is uncertainty about whether similar trends occur over whole-plant canopies or whether canopy-level factors such as leaf area index (LAI) become dominant at this scale. Second, although many ecosystem models simulate plant and soil N dynamics, there are no widely available methods for obtaining mapped foliar N estimates over broad spatial scales. Imaging spectroscopy has been successful for small landscapes (12), but methods that can be applied over larger portions of the globe have not been developed.

Another important means by which ecosystems interact with climate is through biophysical properties such as albedo, which controls the amount of incoming solar radiation that is reflected back to space relative to that which is absorbed and converted to heat. Considerable research has focused on resolving the relative importance of C cycle effects vs. biophysical factors, typically in the context of biome conversions such as deforestation (13, 14). Although results differ among regions, these studies have demonstrated that changes in albedo can be as climatically important as the effects of altered C storage in terms of the overall impact of land cover change on climate (15). To date, most studies have treated albedo and the physiological factors that influence C assimilation as independent mechanisms, and few, if any, have examined the potential for linkages that occur within and among biomes.

Here, we present evidence that the well-known relationship between leaf photosynthesis and foliar N concentrations scales directly to maximum C assimilation over whole-forest canopies and that both variables are strongly and positively correlated with total shortwave surface albedo. Our findings are based on integration of field sampling, high-resolution imaging spectroscopy, broad-band remote sensing, and tower-based CO_2 flux measurements from 12 forested research sites that are distributed across the conterminous U.S. and include a range of forest types (Table 1). We measured whole-canopy N concentrations at 181 field plots, determined as the mean of mass-based foliar %N over all species in each plot (weighted by the relative abundance of each), with samples from >1,700 trees in stands ranging from <15 to >500 years old. Measured %N data were combined in a

Author contributions: S.V.O., A.D.R., M.E.M., and D.Y.H. designed research; S.V.O., A.D.R., M.E.M., D.Y.H., S.E.F., P.B.R., L.C.P., J.W.M., M.-L.S., and M.C.D. performed research; S.V.O., A.D.R., M.E.M., P.B.R., L.C.P., G.G.K., J.W.M., R.O., K.T.P.U., P.V.B., B.D.C., M.C.D., T.A.M., R.K.M., and H.P.S. analyzed data; and S.V.O., A.D.R., D.Y.H., S.E.F., and P.B.R. wrote the paper.

The authors declare no conflict of interest.

Freely available online through the PNAS open access option.

[1]To whom correspondence should be addressed. E-mail: scott.ollinger@unh.edu.

This article contains supporting information online at www.pnas.org/cgi/content/full/0810021105/DCSupplemental.

Table 1. Location and description of the sites used in this work

Site	Lat., °N	Long., °W	Description	Canopy N, % by mass	LAI, m^2 m^{-2}	Age, years
Bartlett Experimental Forest, NH	44°03′	71°17′	Mixed northern hardwood	1.66	4.5	110–130
Donaldson Tract, FL	29°44′	82°13′	Slash pine	0.99	2.9	12
Duke Forest Deciduous, NC	35°58′	79°06′	Oak–hickory	1.85	5.6	90–100
Duke Forest Pine, NC	35°58′	79°05′	Loblolly pine	1.47	4.5	22
Harvard Forest, MA	42°32′	72°10′	Mixed deciduous	1.95	4.9	70
Howland, ME	45°12′	68°44′	Boreal evergreen	1.16	5.7	140
Hubbard Brook, NH*	43°57′	71°44′	Northern hardwoods	2.24	NA†	25
Morgan Monroe State Forest, IN	39°19′	86°24′	Mixed deciduous	2.06	4.9	60–90
Niwot Ridge, CO	40°01′	105°32′	Subalpine evergreen	0.93	4.0	100
Tremper Mount, NY*	42°05′	74°16′	Mixed deciduous	2.35	NA	60–80
Willow Creek, WI	45°48′	90°04′	Temperate deciduous	1.79	5.4	60–80
Wind River Experimental Forest, WA	45°49′	121°57′	Temperate evergreen	0.75	8.2	>500

All but two sites (marked with *) are part of the AmeriFlux research network.
†NA, not available.

partial least squares (PLS) regression with reflectance spectra from NASA's AVIRIS (Airborne Visible/InfraRed Imaging Spectrometer) and Hyperion (aboard the EO-1 satellite) instruments to yield mapped estimates of canopy %N for each site. Canopy %N was calculated for the core area of each tower's daytime footprint (16) by using predicted values from within a 250-m radius circle. A simple model of forest C exchange was combined with daytime CO_2 fluxes to produce estimates of instantaneous, canopy-level photosynthetic capacity (CA_{max}) for the landscape represented by each tower. The model included a function describing the response of photosynthesis to incident photosynthetically active radiation (PAR) and a term for ecosystem respiration, which allowed partitioning of the maximum potential assimilation rate from the tower measurements of net CO_2 exchange.

Results

Across all sites, CA_{max} was highly correlated with canopy %N (Fig. 1). The relationship was slightly stronger when CA_{max} was expressed per unit of canopy leaf mass ($r^2 = 0.76$) rather than per unit of ground area ($r^2 = 0.65$), although both trends were highly significant ($P < 0.01$). The mass-based relationship follows from well-established physiological relations (11), whereas expressing CA_{max} per unit of ground area relates more directly to tower-based measurements and is more relevant for models driven by remotely sensed data. The relationship between mass-based CA_{max} and canopy %N is nearly parallel to the leaf-level relationship between A_{max} and %N for woody plants worldwide (9; Fig. 1*B*). At any given %N, whole-canopy photosynthetic capacity is lower than that for individual leaves, which is expected given the considerable self-shading in multilayered canopies. Neither mass- nor area-based CA_{max} was correlated with LAI ($P > 0.50$ in both cases), likely because most of our study sites are closed canopy forests with relatively high LAI and near-complete interception of available light. Under these conditions, the photosynthetic potential per unit of leaf mass should be a better indicator of the efficiency with which intercepted light is used, rather than the total amount of foliage present. A significant positive relationship between light use efficiency (LUE) under full-sun conditions and canopy %N supports this idea ($P < 0.01$, $r^2 = 0.59$ [see supporting information (SI) Fig. S1 and *SI Text*].

Whereas previous studies have demonstrated the ability to estimate canopy %N over small landscapes by using aircraft-based imaging spectroscopy (12), the scope of our dataset allowed us to examine relationships between %N and reflectance data obtained from global-scale satellite sensors. We systematically degraded the spectral resolution of imaging spectrometer scenes from 10 nm to 20 nm, 30 nm and so on to 100 nm, and repeated the PLS analysis. This process yielded little loss of prediction accuracy, and the reflectance feature that emerged as the dominant source of variability with respect to %N at coarser resolutions was the height of the near-infrared (NIR) reflectance plateau (800–1,200 nm; Fig. 2). We also examined

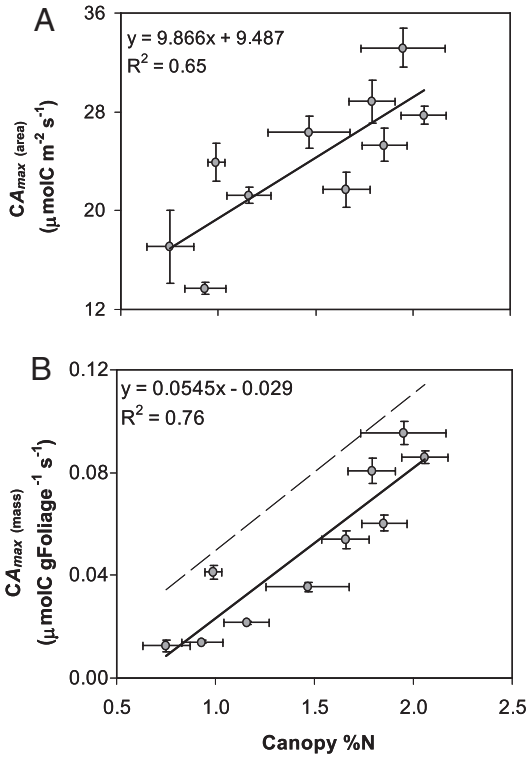

Fig. 1. Relationships among canopy-level CA_{max} and canopy N concentrations (%N) for the eddy covariance towers used in this work ($n = 10$). Area-based CA_{max} (*A*) was derived through inversion of a simple C flux model on tower net CO_2 exchange data. Mass-based CA_{max} (*B*) was derived by combining area-based values with canopy mass estimates for each site. Canopy %N values represent the average of estimates from imaging spectroscopy data, calculated from within a 250-m radius of each tower. The dashed line represents the leaf-level relationship between mass-based A_{max} and %N for woody plants worldwide (9). Uncertainty terms are standard errors of maximum likelihood parameter estimates (CA_{max}) and standard deviations of predicted values from within flux tower footprints (%N).

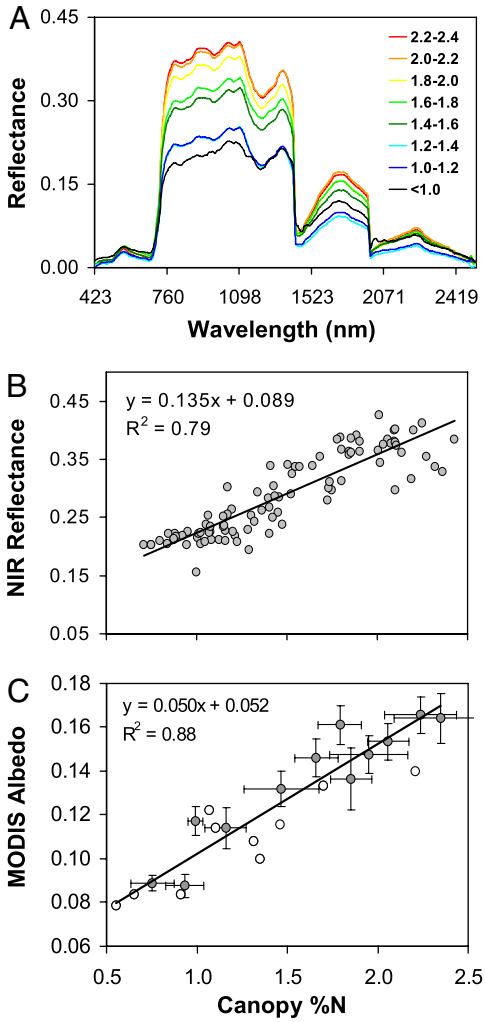

Fig. 2. Relationships between reflectance properties and %N in forest canopies. (*A*) Average AVIRIS reflectance spectra from 102 plots across the study sites, grouped into 10 classes of canopy %N. (*B*) Measured canopy %N in relation to reflectance (ρ) in the near infrared (800–850 nm) spectral range ($P < 0.001$, $n = 102$). ρ was derived by degrading the spectral resolution of AVIRIS and represents a mean of 10-nm bands in the 800- to 850-nm region. (*C*) Canopy %N for flux tower footprints (as in Fig. 1) in relation to shortwave albedo from the MODIS instrument for the peak portion of the growing season. Open symbols are Canadian sites where foliar %N data were available from a prior study (18). Albedo uncertainty terms are standard deviations of all growing season observations between 2000 and 2006.

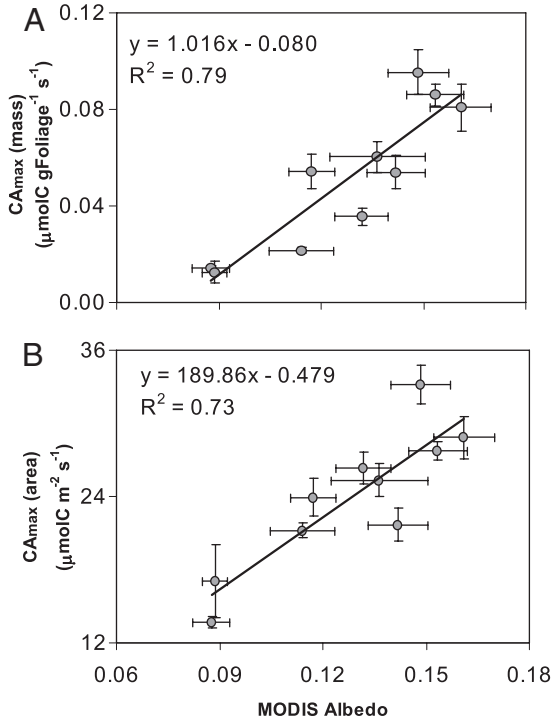

Fig. 3. Shortwave growing season albedo from the MODIS instrument in relation to (*A*) CA_{max} expressed per unit of canopy leaf mass and (*B*) CA_{max} expressed per unit of ground area. Albedo uncertainty terms are standard deviations of all growing season observations between 2000 and 2006.

relationships between %N and common vegetation indices that use NIR to visible reflectance ratios, but none yielded as strong a correlation with measured %N as did NIR reflectance on its own (Fig. 2*B*). The relatively small size of our field plots prevented direct comparison of measured canopy %N with data from coarse-resolution satellite sensors. However, imaging spectrometer %N estimates for the much larger flux tower footprints were positively correlated with NIR reflectance measured at a compatible scale by the MODIS instrument (Moderate Resolution Imaging Spectroradiometer; $r^2 = 0.87$, $P < 0.001$) (see Fig. S2).

As is typical of live vegetation, PAR reflectance (400–700 nm) was lower and less variable than NIR reflectance among all %N classes. At wavelengths >800 nm, however, there was a strong and consistent response of increasing reflectance with increasing %N (Fig. 2*A*). A consequence of this pattern is that canopy %N was significantly correlated with mean reflectance across the entire imaging spectrometer detection range of 400–2,500 nm ($r^2 = 0.69$, $P < 0.001$, $n = 102$). Because full-spectrum reflectance is functionally similar to shortwave albedo, we compared canopy %N with independent estimates of shortwave land surface albedo from MODIS (17) collected during the midgrowing season to match our field sampling. This comparison revealed highly significant relationships between albedo and both canopy %N (Fig. 2*C*) and CA_{max} (Fig. 3). Canopies with high concentrations of N in foliage have both a greater capacity to remove CO_2 from the atmosphere and absorb less incident shortwave radiation than their low-N counterparts. Addition of independent %N data and MODIS albedo values for similarly sized forest landscape units at 8 sites in Canada (18) gives further support to this conclusion and extends the geographic scope and range of values in our data (Fig. 2*C*). As expected, deciduous and evergreen forests tended to separate along high and low portions of the observed trend, respectively, but there is substantial variation within each type, and the %N–albedo relationship is significant for both forest types (deciduous $r^2 = 0.52$, $P < 0.05$, evergreen $r^2 = 0.59$, $P < 0.01$), with no difference in slope or intercept (see *SI Text* for discussion of potential underlying mechanisms for this relationship). Although reflectance properties in forests can also be affected by leaf area and other structural attributes that influence absorbance and scattering within canopies (19), there was no relationship between albedo and either LAI or canopy height when compared individually or in multiple regressions with %N ($P > 0.5$ in all cases; Fig. S3).

Collectively, these results suggest that we already have a basis for detecting variation in %N and CA_{max} of forest canopies at continental scales by using scaled relationships with albedo and/or simple measures of NIR reflectance obtained during the peak period of the growing season. We do not suggest that NIR reflectance and surface albedo are driven solely by canopy %N or related plant traits, but our results do indicate that, for closed

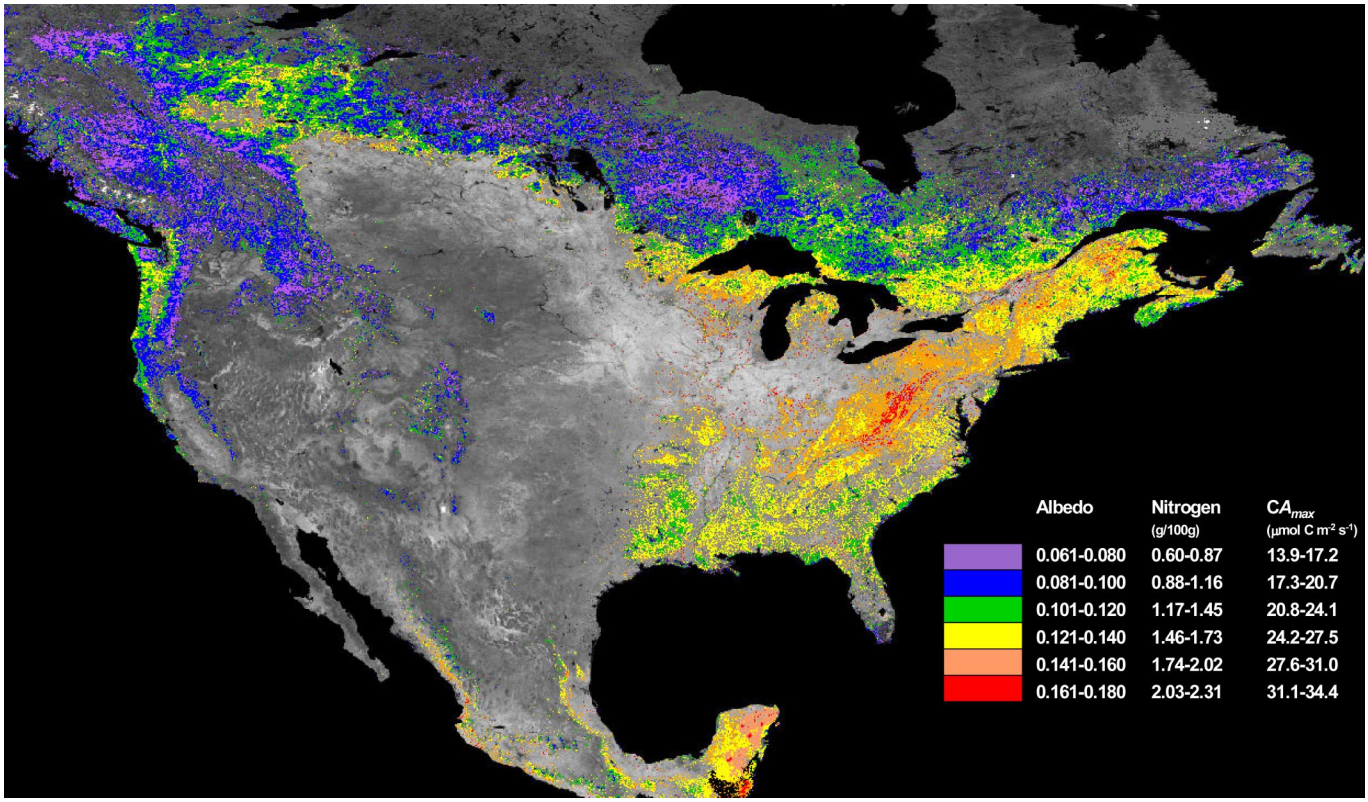

Fig. 4. Estimates of canopy %N and CA_{max} for forested areas of North America, along with the albedo values from which they were derived. Albedo data were from the midportion of the growing season and were converted to estimates of canopy %N and CA_{max} by using trends shown in Figs. 2*C* and 3*B*. Results were applied to forested grid cells only, identified by using the MOD44B continuous vegetation fields data product (41).

canopy temperate and boreal forests, NIR reflectance and albedo patterns are reliably correlated with canopy %N over a wide range of conditions with no underlying influence of variation in LAI. We therefore propose as an initial hypothesis that the dominant patterns of canopy %N and CA_{max} for North American forests can be estimated by combining the trends in Figs. 2*C* and 3*B* with a peak growing season coverage of MODIS shortwave albedo (Fig. 4). Although patterns related to dominant forest functional groups are evident (e.g., higher values in the eastern deciduous biome and lower values in northern evergreens), there is considerable variability within vegetation types, with the highest overall estimates in forests of the mid-Appalachian region. This region has been identified as having high foliar N concentrations relative to other temperate deciduous forests (20, 21), with some evidence that variation is linked to patterns of atmospheric N deposition (21). Additional field measurements can confirm or reject this hypothesis and determine whether or not similar trends can be applied over other regions and vegetation types.

Discussion

The strong linkages among canopy %N, shortwave albedo, and CA_{max} raise the possibility of an unrecognized feedback in the Earth's climate system involving the N cycle as a factor influencing surface energy exchange, in addition to its known effects on C assimilation. As an example, warming trends in boreal and arctic regions result in warmer soils, accelerated decomposition, and increased nutrient mineralization (22). Expected consequences include an increase in the N nutrition of plant canopies (23) or a shift in species composition to those requiring higher N supplies and having higher N concentrations in foliage. Although the effects of changes in major plant functional groups have been included in coupled land surface–climate models (24), those associated with changes in N cycling or shifts in species composition within biomes have not. Based on our findings, these specific changes (i.e., increased N supply or altered composition, both resulting in higher canopy %N) should increase gross C assimilation [and presumably net C sequestration (4, 25)] and surface albedo, both representing negative feedbacks to warming. Similar effects can be expected from anthropogenic N deposition and widespread use of N fertilizers, which also serve to increase canopy %N (26). Conversely, leaf N concentrations in temperate forests are inversely related to mean annual temperature (27) and are driven down by rising CO_2 (6–8), suggesting that temperature and CO_2 increases could lead to reduced canopy albedo and a positive feedback to warming. Additional scenarios can be envisioned, but the overall implication is that alterations to plant N availability have important and unrecognized impacts on the climate system that warrant serious consideration (see *SI Text* for details on surface heating effects over the observed range of %N and albedo). This is particularly relevant in light of the degree to which human activities have altered the N cycle globally (28).

It would be premature to draw management implications from these results or to conclude that N fertilization, increased N pollutant emissions, or shifts from low-N to high-N tree species would help offset climate warming induced by greenhouse gas emissions. We also cannot assume that changes in C assimilation will always lead to a change in net C sequestration, given the potential for synergistic changes in ecosystem respiration. Moreover, interrelations among canopy %N, CA_{max}, and albedo need to be evaluated in additional ecosystem types, particularly in tropical forests, agricultural systems, and ecosystems with low LAI or sparse vegetation cover, and assessing the full outcome

of competing feedbacks will require new analyses using coupled climate–vegetation models. Finally, our analysis did not address N-induced changes in transpiration or potential consequences for cloud formation, which could have important effects on the net change in energy budgets (15) but were beyond the scope of our study. Despite these uncertainties, the observation of strong N–C–albedo linkages in forests add a new dimension to our understanding of the role played by ecosystems within the climate system and warrant consideration in climate projection efforts given the extent to which all of these variables are being altered by human activities.

Methods

Field Sampling. Canopy %N (g of N 100 g of dry leaf matter^{-1}) was sampled between 2001 and 2006 on 181 plots across the 12 research sites used in this study. At each site, plots were chosen from within a 5- × 5-km area to capture ecological variability in forest composition and condition that occurred over the local landscape. At each plot, all dominant and codominant species were identified, and between 2 and 5 trees per species were selected for green leaf collection from several heights in the canopy by using 12-gauge shotguns. Samples were collected to coincide with the peak of the growing season and with overflights by NASA AVIRIS or Hyperion instruments. A benchtop visible and near-infrared spectrophotometer (Foss NIRSystems 6500) was used to determine leaf-level foliar N concentrations of oven-dried, ground foliage according to methods described by Bolster *et al.* (29). The relative abundance of each species in the canopy was determined by using a point intercept sampling technique that quantifies the vertical distribution of leaf mass by species in the canopy (12). Plot-level canopy N concentrations (whole-canopy %N) were calculated as the mean of leaf-level foliar N concentrations among all species, weighted by the mass-based fraction of the canopy represented by each.

Canopy N Remote Sensing. Hyperspectral remote sensing, or imaging spectroscopy, is a form of optical remote sensing in which surface reflectance is examined in narrow and contiguous spectral regions that allow analysis of specific absorption features on a pixel-by-pixel basis. At each site, hyperspectral remote sensing scenes were obtained from NASA's AVIRIS or Hyperion [aboard the Earth Observing-1 (EO-1) satellite] sensors. AVIRIS measures upwelling radiance in 224 contiguous optical bands from 400 to 2,500 nm with a spectral resolution of 10 nm. AVIRIS was flown on an ER-2 aircraft at an altitude of 20,000 m, producing a spatial resolution of 17 m and a swath width of ≈10 km. The Hyperion instrument is part of the NASA EO-1 satellite, which was launched in November, 2000. The Hyperion detection capabilities are similar to those of AVIRIS (220 spectral bands ranging from 400 to 2,500 nm, with a 10-nm spectral resolution) but with a spatial resolution of 30 m. The swath width is 7.5 km, and data are typically collected in 7.5-km × 100-km images. Data from AVIRIS and Hyperion were converted from radiance (W m^{-2} μm^{-1} sr^{-1}) to surface reflectance by using the ACORN atmospheric correction program (ACORN 5.0).

The signal-to-noise ratio of AVIRIS is >600:1 over most of its spectral range, whereas the Hyperion signal-to-noise ratio does not exceed 200:1. For this reason, we used AVIRIS data where possible (9 sites), unless Hyperion was the sole option (3 sites). AVIRIS data yielded full-spectral coverage for all plots, whereas low signal-to-noise resulted in omission of some Hyperion bands. This had little effect on our analysis but may have reduced the accuracy of the Hyperion %N model and prevented full-spectrum average brightness values from being calculated for all plots and scenes.

Detailed methods for deriving canopy %N coverages from AVIRIS and Hyperion are given elsewhere (12). Relationships between plot-level spectra and canopy %N were examined by using PLS regression, in which the full-reflectance spectrum is collapsed into a smaller set of independent variables, or factors, with the measured %N data used directly during the spectral decomposition process. The accuracy of the resulting models was evaluated by using a standard 1-out cross-validation. The PLS models were then used to develop mapped estimates of canopy %N for a 5-km × 5-km landscape centered over each site. Canopy %N for each tower was calculated by using predicted values from within a 250-m-radius circle, corresponding to the core area of a typical tower's daytime footprint (16). Given uncertainties in the actual size of the tower footprints, we also calculated mean %N assuming footprint radii of 500, 750, and 1,000 m. Although the relationships in Fig. 1 generally grew weaker as the assumed footprint radius grew larger, the change was small, and the overall conclusions remained intact (e.g., from 250 m to 1,000 m, the r^2 of mass-based %N vs. CA_{max} declined from 0.72 to 0.58).

Flux Data and Derivation of CA_{max} and LUE Estimates. At each flux tower site, the eddy covariance method (30) was used to obtain continuous measurements of the surface–atmosphere exchange of CO_2, H_2O, and energy. Three years of flux measurements and ancillary meteorological data were used for each site. We used daytime measurements of the net ecosystem exchange of CO_2 (NEE, μmol m^{-2} s^{-1}) to estimate 3 parameters of a simple ''big leaf'' Michaelis–Menten light response model of gross canopy photosynthesis driven by incident solar photosynthetic photon flux density (I, μmol m^{-2} s^{-1}),

$$P_{\text{gross}} = NEE - R_{\text{eco}} = CA_{\text{sat}} \frac{I}{I + K_{\text{m}}} \quad \text{or}$$

$$\text{NEE} = \text{P}_{\text{gross}} + R_{\text{eco}} = CA_{\text{sat}} \frac{I}{I + K_{\text{m}}} + R_{\text{eco}} \qquad [1]$$

where CA_{sat} is the theoretical, whole-canopy light-saturated rate of photosynthesis, K_m is the half-saturation value of I for the light response function, and R_{eco} is ecosystem respiration. Maximum likelihood parameter estimates were fit separately for each site, using 3 years of flux data and a 14-day moving window, following methods described by Press *et al.* (31) and by using flux uncertainty estimates presented by Richardson *et al.* (32). This approach to partitioning NEE to photosynthetic and respiratory component fluxes was recently evaluated and was found to yield results comparable to those of a range of other partitioning methods (33). Because of potential correlation between CA_{sat} and K_m parameters, which could result in unrealistically high values for the theoretical light-saturated rate of uptake, we instead focused subsequent analyses on CA_{max}, the maximum rate of assimilation when I = 2,000 μmol m^{-2} s^{-1}, i.e., under reasonable ''full-sun'' conditions, and when other environmental variables are least limiting. Resulting values for CA_{sat} and CA_{max} were highly correlated ($r^2 = 0.89$, $P < 0.0001$), and use of either variable in the analyses produced the same overall conclusions. The CA_{max} values used for comparison with other variables in the study were means of the peak value achieved during each growing season of the 3-year record.

LAI and Maximum LUE. LAI values were obtained from a combination of published values and measurements taken during the time of our field sampling (34–38). All LAI data were from site-specific, midgrowing season measurements conducted with optically based methods, primarily by using the Li-Cor LAI-2000 (LI-COR Biosciences) instrument. Estimates based on leaf litterfall collections or allometry were also available for some sites. Although small discrepancies among LAI sampling methods have been noted (39), we used data collected from optically based methods to maintain consistency across sites.

Maximum canopy LUE (mol of C assimilated per mol of absorbed photons) was determined by dividing area-based CA_{max} by the quantity of absorbed photosynthetically active radiation (*A*PAR) when I = 2,000 μmol m^{-2} s^{-1}. *A*PAR was estimated by using a simplified model of transmission and scattering of light in plant canopies, applied by using measured LAI values for each site (40).

MODIS Albedo and Surface Reflectance. MODIS reflectance and shortwave albedo data (collection 4, MOD43B4 and MOD43B, respectively) were obtained from the MODIS subset data server for each of the study sites (17). Individual image datasets are 16-day composites of atmospherically corrected surface reflectance, derived by using cloud-free images only. The reflectance product is nadir BRDF-adjusted reflectance (NBAR) and represents reflectance at the mean solar zenith angle. We used reflectance and albedo data from DOY 177 through 241 for years 2001–2006 to calculate mean growing season values that would be compatible with field measurements and hyperspectral imagery. Data completeness for this time period averaged 93% with gaps caused by cloudiness and other data quality issues. Data gaps were distributed randomly in time. Shortwave albedo is calculated across a spectral range of 300–5,000 nm and was available as black-sky, white-sky, and actual albedo (17). Data shown in Fig. 2*C* and 3 are actual albedo, although use of other albedo variables produced nearly identical results (e.g., black-sky values were within 2% of actual albedo, and a regression of the 2 across the study sites produced a relationship with r^2 = 0.997 and a slope and intercept not significantly different from 1 and 0, respectively).

ACKNOWLEDGMENTS. We thank J. Aber, K. Davis, and S. Wofsy for helpful comments on a draft of this manuscript. We thank K. Bible, M. Binford, J. Bradford, S. Burns, C. Costello, D. Dragoni, D. Ellsworth, B. Evans, H. Gholz, J. Jenkins, J. Lee, H. McCarthy, C. Oishi, M. Ryan, C. Schaaf, M. Schroeder, G. Starr, P. Stoy, S. Urbanski, and S. Wharton for help with data collection, distribution, and analysis. We thank Michael Eastwood, Rob Green, and the entire Airborne Visible/InfraRed Imaging Spectrometer flight crew for

image collection and preprocessing. This work was supported the NASA Carbon Cycle Science Program and Interdisciplinary Science Program with contributions from the Harvard Forest, Hubbard Brook, and Cedar Creek Long-Term Ecological Research programs, the U.S. Department of Agriculture Forest Service Northern Research Station, the Northeastern States Research Cooperative and the U.S. Department of Energy Office of Science (BER) through the Northeastern Regional Center of the National Institute for Climatic Change Research.

1. Heimann M, Reichstein M (2008) Terrestrial ecosystem carbon dynamics and climate feedbacks. *Nature* 451:289–292.
2. Houghton RA (2007) Balancing the global carbon budget. *Annu Rev Earth Planet Sci* 35:313–347.
3. Schimel D, *et al.* (2000) Contribution of increasing CO_2 and climate to carbon storage by ecosystems in the United States. *Science* 287:2004–2006.
4. Magnani F, *et al.* (2007) The human footprint in the carbon cycle of temperate and boreal forests. *Nature* 447:848–850.
5. LeBauer DS, Treseder KK (2008) Nitrogen limitation of net primary productivity in terrestrial ecosystems is globally distributed. *Ecology* 89:371–379.
6. Oren R, *et al.* (2001) Soil fertility limits carbon sequestration by forest ecosystems in a CO_2-enriched atmosphere. *Nature* 411:469–472.
7. Ainsworth EA, Long SP (2005) What have we learned from 15 years of free-air CO_2 enrichment (FACE)? A meta-analytic review of the responses of photosynthesis, canopy properties, and plant production to rising CO_2. *New Phytol* 165:351–372.
8. Reich PB, Hungate BA, Luo Y (2006) Carbon–nitrogen interactions in terrestrial ecosystems in response to rising atmospheric carbon dioxide. *Annu Rev Ecol Evol System* 37:611–636.
9. Wright IJ, *et al.* (2004) The worldwide leaf economics spectrum. *Nature* 428:821–827.
10. Field C, Mooney HA (1986) The photosynthesis–nitrogen relationship in wild plants. *Proceedings of the Sixth Maria Moors Cabot Symposium, Evolutionary Constraints on Primary Productivity: Adaptive Patterns of Energy Capture in Plants, Harvard Forest, August 1983*, Givnish TJ, ed (Cambridge Univ Press, Cambridge, UK), pp 25–55.
11. Reich PB, *et al.* (1999) Generality of leaf trait relationships: A test across six biomes. *Ecology* 80:1955–1969.
12. Ollinger SV, Smith M-L (2005) Net primary production and canopy nitrogen in a temperate forest landscape: An analysis using imaging spectroscopy, modeling and field data. *Ecosystems* 8:760–778.
13. Betts RA (2000) Offset of the potential carbon sink from boreal forestation by decreases in surface albedo. *Nature* 408:187–190.
14. Bala G, *et al.* (2007) Combined climate and carbon-cycle effects of large-scale deforestation. *Proc Natl Acad Sci USA* 104:6550–6555.
15. Bonan GB (2008) Forests and Climate Change: Forcings, Feedbacks, and the Climate Benefits of Forests. *Science* 320:1444–1449.
16. Schmid HP (2002) Footprint modeling for vegetation atmosphere exchange studies: A review and perspective. *Agric For Meteorol* 113:159–183.
17. Schaaf CB, *et al.* (2002) First operational BRDF, albedo nadir reflectance products from MODIS. *Remote Sens Env* 83:135–148.
18. Schwalm CR, *et al.* (2006) Photosynthetic light use efficiency of three biomes across an east–west continental-scale transect in Canada. *Agric For Meteorol* 140:269–286.
19. Asner GP (1998) Biophysical and biochemical sources of variability in canopy reflectance. *Remote Sens Env* 64:234–253.
20. Townsend PA, Foster JR, Chastain RA, Jr, Currie WS (2003) Application of imaging spectroscopy to mapping canopy nitrogen in the forests of the central Appalachian Mountains using Hyperion and AVIRIS. *IEEE Trans Geosci Remote Sens* 41:1347–1354.
21. Boggs JL, McNulty SG, Gavazzi MJ, Myers JM (2005) Tree growth, foliar chemistry, and nitrogen cycling across a nitrogen deposition gradient in southern Appalachian deciduous forests. *Can J For Res* 35:1901–1913.
22. Hinzman LD, *et al.* (2005) Evidence and implications of recent climate change in northern Alaska and other Arctic regions. *Climatic Change* 73:251–298.
23. Melillo JM, *et al.* (2002) Soil warming and carbon-cycle feedbacks to the climate system. *Science* 298:2173–2176.
24. Friedlingstein P, *et al.* (2006) Climate–carbon cycle feedback analysis: Results from the C^4MIP model intercomparison. *J Climate* 19:3337–3353.
25. Law BE, *et al.* (2002) Environmental controls over carbon dioxide and water vapor exchange of terrestrial vegetation. *Agric For Meteorol* 113:97–120.
26. Magill AH, *et al.* (2004) Ecosystem response to 15 years of chronic nitrogen additions at the Harvard Forest LTER, Massachusetts, USA. *For Ecol Manage* 196:7–28.
27. Yin X (1992) Empirical relationships between temperature and nitrogen availability across North American forests. *Can J For Res* 22:707–712.
28. Gruber N, Galloway JN (2008) An Earth-system perspective on the global nitrogen cycle. *Nature* 451:293–296.
29. Bolster KL, Martin ME, Aber JD (1996) Determination of carbon fraction and nitrogen concentration in tree foliage by near infrared reflectances: A comparison of statistical methods. *Can J For Res* 26:590–600.
30. Baldocchi DD (2003) Assessing the eddy covariance technique for evaluating carbon dioxide exchange rates of ecosystems: Past, present and future. *Global Change Biol* 9:479–492.
31. Press WH, Flannery BP, Teukolsky, SA, Vetterling WT (1992) *Numerical Recipes in Fortran 77: The Art of Scientific Computing* (Cambridge Univ Press, New York).
32. Richardson AD, *et al.* (2006) A multi-site analysis of random error in tower-based measurements of carbon and energy fluxes. *Agric For Meteorol* 136:1–18.
33. Desai AR, *et al.* (2008) Cross-site evaluation of eddy covariance GPP and RE decomposition techniques. *Agric For Meteorol* 148:821–838.
34. Curtis PS, *et al.* (2002) Biometric and eddy covariance-based estimates of annual carbon storage in five eastern North American deciduous forests. *Agric For Meteorol* 113:3–19.
35. Cohen WB, *et al.* (2003) Comparisons of land cover and LAI estimates derived from ETM+ and MODIS for four sites in North America: A quality assessment of 2000/2001 provisional MODIS products. *Remote Sens Env* 88:233–255.
36. Cook BD, *et al.* (2004) Carbon exchange and venting anomalies in an upland deciduous forest in northern Wisconsin, USA. *Agric For Meteorol* 126:271–295.
37. Parker GG, *et al.* (2004) Three-dimensional structure of an old-growth Pseudotsuga–Tsuga canopy and its implications for radiation balance, microclimate, and gas exchange. *Ecosystems* 7:440–453.
38. Turnipseed AA, Blanken PD, Anderson DE, Monson RK (2002) Energy budget above a high-elevation subalpine forest in complex topography. *Agric For Meteorol* 110:177–201.
39. Asner GP, Scurlock JMO, Hicke JA (2003) Global synthesis of leaf area index observations: Implications for ecological and remote sensing studies. *Global Ecol Biogeog* 12:191–205.
40. Norman JM, Campbell GS (2007) Canopy structure. *Plant Physiological Ecology: Field Methods and Instrumentation*, Pearcy RE, Ehleringer JR, Mooney HA, Rundel PW, eds (Chapman and Hall, London), pp 301–325.
41. Hansen MC, *et al.* (2003) Global percent tree cover at a spatial resolution of 500 meters: First results of the MODIS vegetation continuous fields algorithm. *Earth Interactions* 7:1–15.